RESEARCH ARTICLE

Comparison and Evaluation of the Effectiveness of Two Approaches of Diffusible Iodine-Based Contrast-Enhanced Computed Tomography (diceCT) for Avian Cephalic Material

ZHIHENG LI[1]*, RICHARD A. KETCHAM[1], FEI YAN[2], JESSICA A. MAISANO[1], AND JULIA A. CLARKE[1]

[1]Department of Geological Sciences, The University of Texas, Austin, Texas
[2]Department of Civil and Environmental Engineering, Rice University, Houston, Texas

ABSTRACT

Diffusible iodine-based contrast-enhanced computed tomography presents a comparatively new tool kit for imaging fine-scale three-dimensional phenotypes that is rapidly becoming standard anatomical practice. However, relatively few studies have attempted to look at subtle differences in staining protocols or attempted to model tissue reactions to gain insight into staining mechanisms. Here, two iodine-based contrast agents, iodine-ethanol (I_2E) and iodine-potassium iodide (I_2KI) in neutral buffered formalin , were applied to avian cephalic specimens to investigate their effectiveness. We found that the two solutions had markedly different results for staining of mineralized skeletal tissues (i.e., bone). Other tissues, including muscles, epithelia, and common connective tissues (e.g., lamina propria) were assessed individually and show minor differences in the sorption of iodine. Numerical simulations suggest that different results from I_2E and I_2KI-formaldehyde staining are due to different partition coefficients and retardation factors of tissues, fixation effects, as well as distinct iodine diffusion and sorption patterns. We found a clear positive relationship between glycogen concentration and grayscale values measured within muscle, epithelia, nervous tissues, and glands. We also found the use of ethanol for tissue fixation and following I_2E staining outperforms I_2KI-formaldehyde by providing higher efficiency for acquiring greater contrast both between different soft tissues and between mineralized and nonmineralized tissues. *J. Exp. Zool. (Mol. Dev. Evol.) 326B:352–362, 2016.* © 2016 Wiley Periodicals, Inc.

All the authors have read the paper and have agreed to have their names listed as authors.
Contract grant sponsor: Gordon and Betty Moore Foundation; Contract grant no. 4498; Contract grant sponsor: Jackson School of Geosciences, The University of Texas at Austin; Contract grant sponsor: NSF; Contract grant number: EAR-1258878.
Conflict of interest: None.
Additional Supporting Information may be found in the online version of this article.
*Correspondence to: Zhiheng Li, Jackson School of Geosciences, Department of Geological Sciences, The University of Texas at Austin, 2275 Speedway Stop C9000, Austin, TX 78712.
E-mail: lizhiheng1982@hotmail.com
Received 16 March 2016; Revised 8 June 2016; Accepted 18 June 2016
DOI: 10.1002/jez.b.22692
Published online 11 August 2016 in Wiley Online Library (wileyonlinelibrary.com).

J. Exp. Zool. (Mol. Dev. Evol.) 326B:352–362, 2016

How to cite this article: Li Z, Ketcham RA, Yan F, Maisano JA, Clarke JA. 2016. Comparison and evaluation of the effectiveness of two approaches of diffusible iodine-based contrast-enhanced computed tomography (diceCT) for avian cephalic material. J. Exp. Zool. (Mol. Dev. Evol.) 326B:352–362.

Both iodine-potassium iodide (I_2KI) and iodine-ethanol (I_2E) have been reported as effective in staining organic materials for computed tomography (CT) analysis to aid in capturing three-dimensional anatomy in an array of specimens (Metscher, 2009a,b; Holliday et al., 2013; Gignac and Kley, 2014; Gignac et al., 2016). Iodine, the most common contrast agent, is used in two types of preparation and subsequent staining, commonly referred to as the I_2E and I_2KI approaches (Metscher, 2009a,b). Both are based on the idea of increasing solubility of molecular iodine in solutes, although in different ways (Metscher, 2009a,b). The aqueous I_2KI or so-called Lugol's iodine is prepared by adding one unit (mass) of elemental iodine (I_2) with two units of potassium iodide (KI) into a certain amount of aqueous solution (Gray, '54). Various concentrations (1–20% w/v) of Lugol's iodine have been adopted in different studies (Metscher, 2009a,b; Holliday et al., 2013; Gignac and Kley, 2014; Gignac et al., 2016). The two solutes (i.e., I_2, KI) react and form K^+–I_3^- bonds in the solution (Degenhardt et al., 2010). The products purportedly synthesized through this process include not only I_3^- but also I_5^- and possibly other more complex iodide species (Yu et al., '96). These products are all soluble in water or other aqueous-based solutions (e.g., 10% neutral buffered formalin [NBF]). In contrast, I_2E solution is typically prepared by adding elemental iodine directly into pure ethanol (≥99.5%) (Metscher, 2009a,b). Previous results have indicated that the two approaches are equally effective for the staining of small organic specimens, including both plants and animals (Metscher, 2009a,b; Staedler et al., 2013).

Prestaining preparation differs when using I_2KI or I_2E as the dissolution of iodine varies by solvent. For instance, iodine has a much higher solubility in ethanol than in water (Varlamova et al., 2009). Therefore, the I_2E approach requires an intermediate step of transferring the specimen to pure ethanol (usually ≥99.5%) prior to staining; this step removes extra water in the specimen, which was previously fixed either in aqueous formalin, or in 70% ethanol solution, or both. The I_2KI approach does not require additional preparation aside from using NBF (10%) for fixation. Transferring the fixed specimen into water before staining is suggested but may not be necessary (Li et al., 2015).

Even though the two preparations and respective staining procedures are widely utilized, the specific ways in which they cause iodine to react with tissues remains unclear, and their comparative efficacy for staining distinct tissue types has not been explored in detail. Here, we compare and systematically evaluate two methods (I_2KI-formaldehyde and I_2E treatments) of diffusible iodine-based contrast-enhanced computed tomography (diceCT; Gignac et al., 2016) for staining tissues of the head and tongue of a paleognathous bird, the Chilean Tinamou (*Nothoprocta perdicaria*). Our comparison addresses major tissue types, including epithelia, connective tissues, nervous tissues, and muscle tissues, for their reactions to iodine. We also carry out simulations to explore the key factors that affect iodine diffusion and sorption patterns within three different tissues under the I_2KI-formaldehyde and I_2E treatments. Finally, we discuss potential causes for staining differences and the observed efficiency of the different fixation approaches and present guidelines for which approach may be best given a specific sample and research question.

MATERIALS AND METHODS

Specimen Processing

Four farm-raised Chilean Tinamou specimens were acquired by T. Riede and F. Goller for the Utah Museum of Natural History in Salt Lake City (UMNH). Two of these specimens were decapitated, one between cervical four and five and the other between five and six. The tongue and trachea were dissected out of the other two specimens and stained separately. All specimens were treated and scanned at The University of Texas at Austin.

For the I_2KI-formaldehyde approach, the cephalic specimen (UMNH 23838) was first fixed in 10% NBF for 4 days, and then stained in a stepwise pattern by progressively increasing the concentration of freshly prepared staining solution (1–3% w/v). The 1% w/v (0.5 g I_2 + 1 g KI)/(150 mL NBF), 2% w/v (2 g I_2 + 4 g KI)/(300 mL NBF), and 3% w/v (2 g I_2 + 4 g KI)/(200 mL NBF) I_2KI solutions were used for 6, 12, and 13 days, respectively. The tongue specimen (UMNH 23840) was processed in the same manner as the head for fixation, and then stained using 1% w/v I_2KI-NBF solution for 7 days and 2% w/v I_2KI-NBF for 17 days. The use of formalin as our staining solution rather than deionized water is based on the long period required for adequate staining of the large specimens in this study compared to the size of material used by most previous authors (Metscher 2009a,b; Gignac and Kley, 2014; Gignac et al., 2016). Although the use of formalin might reduce the diffusion rates of triiodide (I_3^-) in the solution, potential advantages of this approach are increasing the fixation effects, better preservation of tissues, and prevent the degradation during the long staining period.

For the I_2E approach, two specimens were NBF fixed then transferred to 70% ethanol for preservation for approximately 1 year. Before staining, the cephalic material (UMNH 23837) was transferred into pure ethanol solution (≥99.5%) for 2 days and then immersed in 1% w/v I_2E (2 g iodine/200 mL pure ethanol, ≥99.5%) for 29 days. The solution was replaced with new 1%

Table 1. X-ray computed tomography scanning parameters

Scanning parameters	Head A (UMNH 23838) (I_2KI-formaldehyde processed)	Head B (UMNH 23837) (I_2E processed)	Tongue A (UMNH 23840) (I_2KI-formaldehyde processed)	Tongue B (UMNH 23839) (I_2E processed)
Voltage (kV)	120	120	70	70
Current (mA)	10	10	10	10
Detector (mm)	74.3	74.3	55	65.5
Source (mm)	−126	−126	−57.5	−57
Voxel size (μm)	42.39	42.30	34.38	31.30
Total slices (number)	1,518	1,355	2,581	2,616

w/v I_2E on day 14. The dissected tongue and trachea from specimen UMNH 23839 was dehydrated for 2 days using pure ethanol and then stained using 0.4% w/v I_2E for 10 days. The dehydration period is partially size dependent, which was determined based on previous successful trials (Riede et al., 2015). Pre-preservation in 70% ethanol for 1 year or more is not necessarily part of the protocol design described here. However, it is worth noting that most museum specimens will have a similar history, that is, NBF fixed and subsequently stored in 30–70% ethanol for many years.

Previous studies have indicated that the concentration of a staining solution can be optimized by considering the sample volume and its surface area (Gignac and Kley, 2014; Gignac et al., 2016); lower concentrations and shorter immersion times were appropriate for the tongue specimens treated relative to the larger cephalic specimens. In this study, quantitative comparisons are made only for the two cephalic specimens (UMNH 23837 and UMNH 23838) and not the tongues, because the tongues were processed using different iodine concentrations and staining durations as described above, and thus staining results can only be qualitatively compared.

X-Ray CT Imaging and Grayscale Measurements

All prepared specimens were scanned using the microXCT 400 scanner (built by Zeiss, formerly Xradia, Inc.) at the High-Resolution X-ray Computed Tomography Facility (UTCT) at the University of Texas at Austin. Scanning parameters were the same for the cephalic and tongue samples (Table 1), with slight adjustments to optimize the voxel size for one tongue sample. Reconstruction parameters were identical among the heads but not the dissected tongues; this is another reason quantitative comparison of grayscale values between the tongue specimens was not made. The use of identical parameters for the two cephalic specimens was intended to allow grayscale differences between fully stained tissues to be interpreted as absolute differences due to the two staining approaches.

All datasets were reconstructed as 16-bit TIFF images. Measurements were performed on these images using the Analyze Histogram function in ImageJ (v1.49). As grayscale values varied for a specific tissue in the specimen, we selected a region for the measurement with similar position in both heads (see the Supporting Information Material for measurement locations); both the mean and standard deviation are provided in Figure 1 (see Supporting Information Material for raw data). Our measurements are informative in terms of reflecting the major differences in I_2KI-formaldehyde and I_2E staining, although there might be minor variations in grayscale values across different sections due to beam hardening.

Simulations

A simplified one-dimensional diffusion–sorption (D–S) model was used to simulate the diffusion and sorption process of I_2KI-formaldehyde (Li et al., 2015) and I_2E in the avian cranial samples. A linear sorption isotherm was assumed in this study (Yan et al., 2015). The transport of I_2E/I_2KI-formaldehyde is described by the following equation:

$$(\theta + \rho_b * K_d)\frac{\partial c}{\partial t} = \theta * D\frac{\partial^2 c}{\partial x^2} \quad (1)$$

where θ is porosity (0–1), ρ_b is bulk density (kg/L), D is diffusion coefficient (m^2/s), and the partition coefficient K_d describes the sorption of I_2E/I_2KI-formaldehyde between solid phase (tissue) and solute phase (i.e., $K_d = c_{solid}/c$). The retardation factor R_t is defined as $(1 + \rho_b K_d/\theta)$, and equation (1) is simplified to

$$\frac{\partial c}{\partial t} = \frac{D}{R_t} * \frac{\partial^2 c}{\partial x^2} \quad (2)$$

Here, D/R_t represents the effective diffusion coefficient. It equals the diffusion coefficient of a chemical obtained under nonadsorbing conditions divided by a retardation factor of the adsorbing system (Shackelford and Daniel, '91). Three different tissues (skin, muscle, and fascia) were present in the cervical

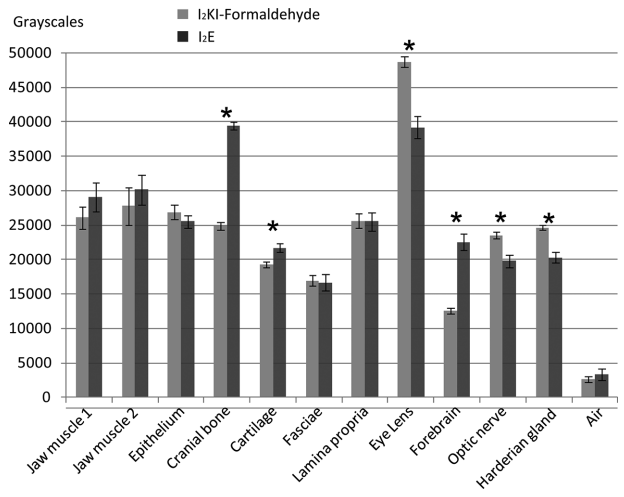

Figure 1. Comparative grayscale values for different tissues measured for the two cephalic specimens with standard deviation (narrow bar). Measurements of tissue grayscales showing statistically significant differences for the two approaches are highlighted with asterisks. Note that the cranial bone and cartilage stain more intensely (show higher grayscale values) in the I_2E staining, whereas the lens and Harderian gland show a higher staining effect with the I_2KI-formaldehyde approach. Measurement locations are given in the Supporting Information Material.

region of the cephalic samples (Supporting Information Material) and the grayscale range of each tissue was determined by visual inspection and measurements of the CT images. To generate iodine concentration profiles, the grayscales of diffusion domains in the cervical region were measured using Plot Profile (ImageJ v1.49) along the selected line in the CT images. The measurements (grayscales) were normalized to "iodine concentration" by dividing them by the grayscales of staining solution trapped within the orbit, and then multiple the ratio by the concentration of staining solution. Here, we assume that the concentration changes in the staining solution are trivial because of the large volume of solution used in comparison to the size of the sample being stained. In addition, the refreshment of staining solution is intended to maintain the solution concentration.

Specific parameters were assigned as priors for the porosity and bulk density of three tissues modeled (Table 2). The diffusion coefficient was considered to be a constant value in each zone of the two systems (I_2E/I_2KI-formaldehyde). The sorption of iodine for different soft tissues is different in both systems, and the partition coefficient (K_d) of each tissue type is also variable in both systems (Li et al., 2015). K_d of each zone (or each tissue), therefore, is calibrated by fitting the model to observations (i.e., iodine concentration profile). We assumed a constant flux (N_{bc}) at the boundary between skin and solution, which needs to

Table 2. Diffusion parameter assumption (θ, ρ_b, D) and calibrated results (Flux, K_d) in the diffusion–sorption modeling

	Target domain	Range (mm)	Porosity (θ)	Bulk density-ρ (kg/L)	Partition coefficient (K_d, L/kg)	Retardation factor (R_f)	Initial concentration (mmol/L)	D (m^2/sec)	Flux (N_{bc}) (m·mmol/(L·sec))
I_2KI-formaldehyde	Zone 1 (skin)	0.55–1.02	0.3	0.75	12.3	31.75	0	1×10^{-9}	9.5×10^{-7}
	Zone 2 (muscle)	1.02–4.32	0.75	0.315	38	16.96			
	Zone 3 (fascia)	4.32–4.62	0.67	0.23	38	14.045			
	Zone 4 (muscle)	4.62–7.60	0.75	0.315	38	16.96			
I_2E	Zone 1 (skin)	1.06–1.29	0.3	0.75	4.1	11.25	0	1×10^{-9}	5.7×10^{-7}
	Zone 2 (muscle)	1.29–1.50	0.75	0.315	9	4.78			
	Zone 3 (fascia)	1.50–1.63	0.67	0.23	8.5	3.918			
	Zone 4 (muscle)	1.63–7.00	0.75	0.315	9	4.78			

Density and porosity of tissues are consulted from literature (ICRP, 2009, Zaidi and Lanigan, 2010; Schleip and Müller, 2013). See Supporting Information Material from where measurements of the concentration profile were taken in the CT images.

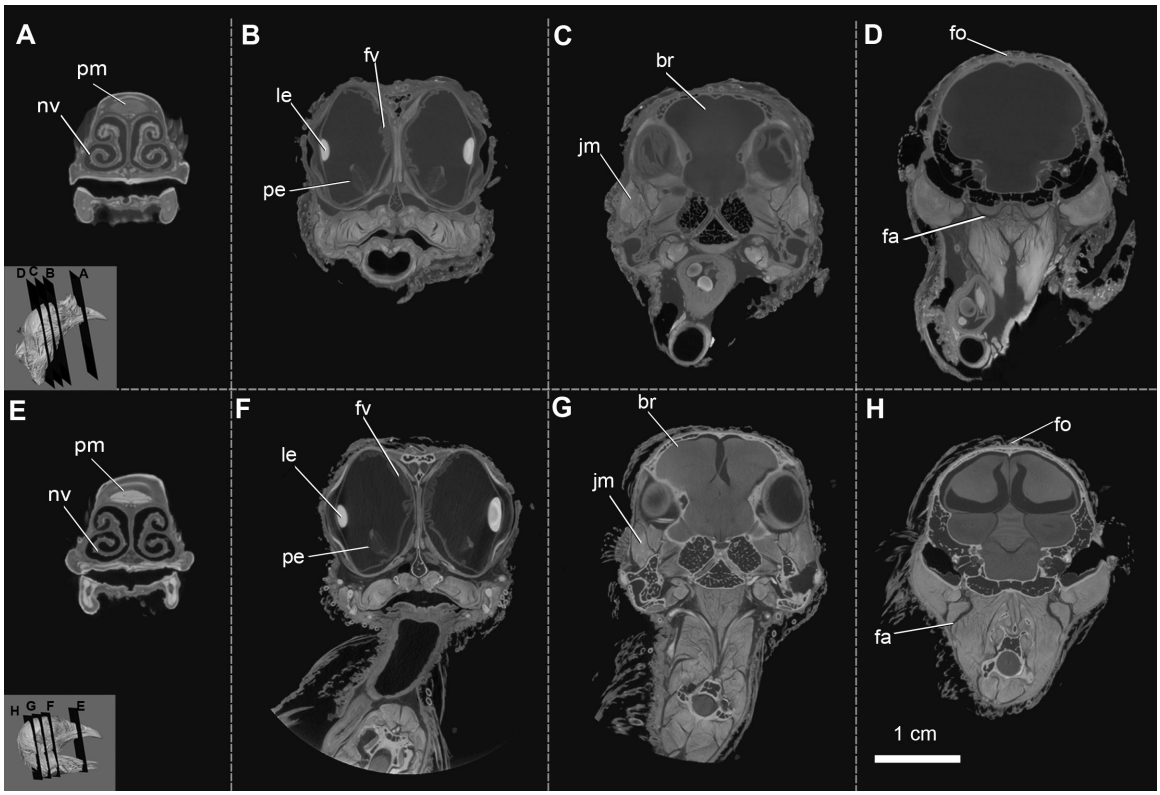

Figure 2. Coronal sections of the two Chilean Tinamou heads processed using I_2KI-formaldehyde solution (A–D, UMNH 23838, male) and I_2E (E–H, UMNH 23837, female), respectively, with the coronal sections indicated in the insects with the 3D renderings for each specimen in (A) and (E). br, brain; fa, fasciae; fo, follicle; fv, fovea; jm, jaw muscle; le, lens; nv, nasal valve; pe, pecten; pm, premaxilla.

be calibrated, to simplify the model. The boundary flux at the inside domain is set as 0. The initial concentration c is set as zero in the model. Simulations by the D–S model were implemented using COMSOL Multiphysics, and four parameters (K_d for the skin, muscle, and fascia, and flux N_{bc}) were calibrated by fitting the model to experimental measurements in the I_2E and I_2KI-formaldehyde systems.

Glycogen–Grayscale Relationship

Glycogen is one of the major common absorbents of iodine that potentially raises the radiographic contrast during staining (Lecker et al., '97; Jeffery et al., 2011; Li et al., 2015). We hypothesized that the proportion of glycogen content in a given tissue is a key factor in determining its maximal grayscale values (absorption). Data were collected from the literature for four tissues with varying glycogen concentrations, that is, Harderian gland, oral epithelium, skeletal muscle, and optic nerve (Brobby, '72; Hevor et al., '75; Isacsson and Mervyn, '81; Lewis, 2004). The relationship between glycogen content and their respective grayscale values was further evaluated.

RESULTS

Comparison of Staining Effects

In the I_2KI-formaldehyde-treated specimen, ossified bony tissues are negligibly affected. Eventually, with sufficient sorption of the stain, the grayscales of muscles approached or even exceeded those of nearby bones (Figs. 1–3), reversing the typical X-ray contrast between nonmineralized and mineralized tissues (Figs. 2 and 3). By contrast, in the I_2E approach, a dramatic increase in grayscale values in ossified tissues occurred along with other tissue types; this increase occured both spongy and compact bones (Fig. 2). In the I_2E approach, therefore, the distinct contrast between mineralized and nonmineralized tissues remained even though other soft tissues were also highly stained, as seen in both the heads and tongues (Figs. 2 and 3). Consistent with the clear visual contrast, bones have much higher measured grayscale values measured after I_2E treatment, 39,432 ± 619, as opposed to only 24,833 ± 575 for the same bone with I_2KI-formaldehyde staining (Fig. 1).

Grayscale values of the lingual cartilage (i.e., paraglossal) in the intact cephalic specimens are lower in I_2KI-formaldehyde

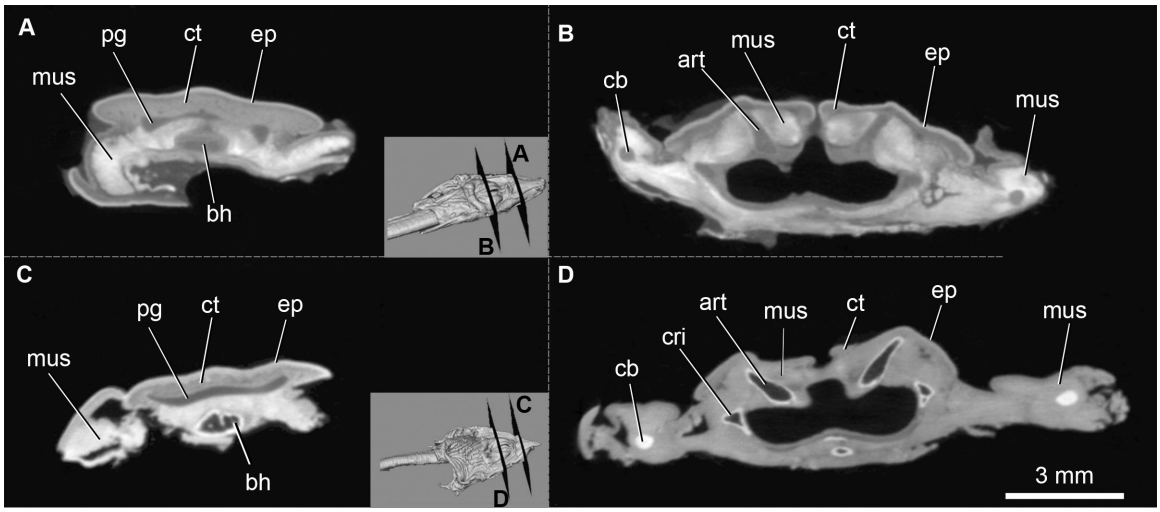

Figure 3. Coronal sections of the two tongue specimens treated with I_2KI-formaldehyde (A and B, UMNH 23840, male) and I_2E (C and D, UMNH 23839, female), respectively. art, artinoid; bh, basihyal; cb, ceratobranchial; cri, cricoid; ct, connective tissue; ep, epithelium; mus, muscle; pg, paraglossal. Inset 3D renderings for each specimen show the section positions in (A) and (C).

(19,232 ± 413) than with I_2E staining (21,714 ± 632). These values are much lower than other stained tissues, and only higher than the fasciae (Fig. 1). The lower grayscale values observed in cartilage distinguish them from the more highly stained muscles or epithelia in both staining method (Fig. 3A and C). Similar to cartilage, fascia is also distinct in its much lower grayscale values, although immersion was rather long compared to other studies (Jeffery et al., 2011; Li et al., 2015). Because major fasciae delineate the orientation of specific muscular fibers, their differentiation provides essential information regarding the muscular bands (Fig. 2). Iodine sorption capacity of nonmineralized connective tissues (e.g., fasciae) is much less than that of other soft tissues, although they are quite permeable to I_2KI-formaldehyde and I_2E solution.

The I_2KI-formaldehyde and I_2E approaches show similar results in epithelia staining, as seen in the nasal capsule, lingual, and esophageal epithelium (Fig. 2). Grayscale values of both the lingual and esophageal epithelia are similar in the two approaches (Fig. 1), even though the solutions have different molar concentrations of iodine. Given extensive staining, similar grayscale values of the esophageal epithelia (26,855 ± 1,057 vs. 25,538 ± 940) indicate their similarly maximum capacity for iodine sorption in I_2KI-formaldehyde solution and I_2E.

The two approaches have consistently yielded equally satisfactory effects for muscular staining (Figs. 1–3; Metscher, 2009a,b; Jeffery et al., 2011; Holliday et al., 2013; Gignac and Kley, 2014; Gignac et al., 2016). These results suggest a high iodine sorption capacity (I-I, I_3^-, I_5^-) in the major component of muscles, the myocytes or glycogen, and lipids (Palumbo and Zullo, '87; Lecker et al., '97; Li et al., 2015). Except for the eye lens, stained muscular tissues have the highest grayscale values (Fig. 1). Although the I_2KI-formaldehyde solution used here has a higher iodine molar concentration than the I_2E (Fig. 1), slightly higher grayscale values of muscle were observed from I_2E staining (Fig. 1). This result was confirmed by the muscles in the neck region as well (Supporting Information Material).

The optic nerve, brain, and spinal cord show the potential to be stained in both the I_2KI-formaldehyde and the I_2E solutions, but to different degrees. Staining of the deep brain tissue is significantly different between the two approaches (Fig. 1). The I_2KI-formaldehyde treatment showed inefficient penetration through the cranium, as indicated by the nonvarying grayscale values across the interior brain. Because of direct contact with the solution, the spinal cord close to the severed edge was clearly stained, but not to the occipital region. A gradual decrease in grayscale values along the spinal cord cranially was shown (Fig. 4: black arrow). In comparison to I_2KI-formaldehyde staining outcomes, the central nervous tissue is much more time efficiently stained when using I_2E; this is mainly due to an efficient penetration of iodine through the highly mineralized bone (Fig. 4). The optic nerves, in direct contact with solution through the optic foramen, are effectively stained by both I_2KI-formaldehyde and I_2E. Their grayscale values are higher in I_2KI-formaldehyde solution staining (23,542 ± 482) than using I_2E (19,783 ± 919). Grayscale variability observed is consistent with the different concentrations of solution used (Fig. 1).

Prior to staining, all avian cephalic tissues exhibit very similar X-ray attenuation except bone, which has a much higher density

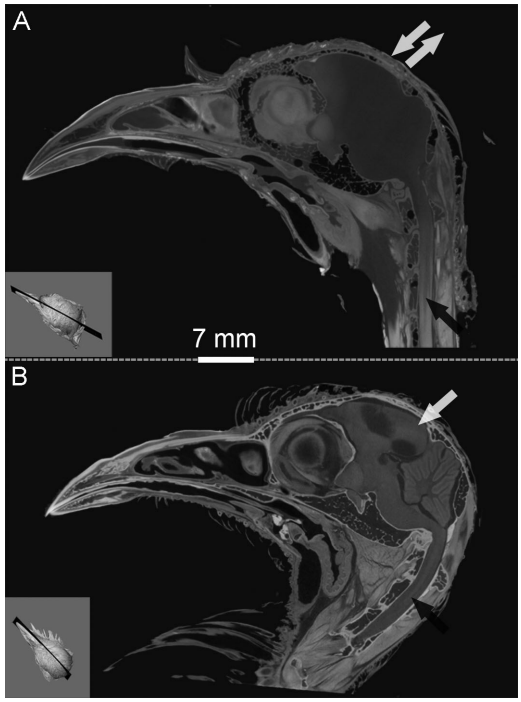

Figure 4. Sagittal sections of the two tinamou heads processed using I_2KI-formaldehyde (A, UMNH 23838, male) and I_2E (B, 23837, female), respectively. Black arrows highlight the staining effect on the spinal cord; white arrows highlight the differential penetration of iodine in the two approaches (iodine was obstructed in (A) by the cranial bone, but penetrated through in (B)). Inset 3D renderings for each specimen show the section positions.

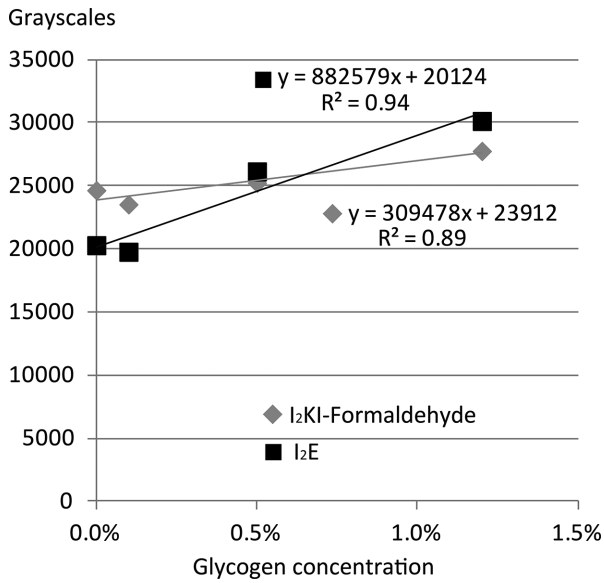

Figure 5. The relationship between glycogen concentration and grayscale values measured in I_2KI-formaldehyde and I_2E staining. The tissues used are representatives of Harderian gland, epithelium, skeletal muscle, and optic nerve. The glycogen concentrations for these tissues are 0, 0.5, 1.2, and 0.1% (w/w), whose values are adopted from references (Brobby, '72; Hevor et al., '75; Isacsson and Mervyn, '81; Lewis, 2004). Here, we use data from the optic lobe for the optic nerve and from human oral epithelial tissues instead of avian tissues due to the lack of available data. The tissue mean grayscale values were measured in ImageJ (v1.49).

due to its compact mineralized structure (Steiniche and Hauge, 2003). The radiographic contrast after iodine staining among different tissues is caused by their variable sorption capacities for different iodine species, given adequate staining duration. Therefore, the grayscale values for different stained tissues can fairly represent their maximal absorptive capacity while approaching iodine saturation. Grayscale values are greatest in the eye lens, followed by the skeletal muscles and epithelia, and least in the nervous and connective tissues. Four types of soft tissues were chosen here for quantitative comparison of their grayscale values in relationship to glycogen content. A positive relationship between glycogen concentration and grayscale values in these tissues is confirmed in both the I_2KI-formaldehyde and I_2E system, although with different slopes (Fig. 5). The steeper slope of the plot for the I_2E system indicates for a similar duration and lower concentration, major soft tissues compared here have a greater disparity in their grayscale values than those stained with the I_2KI-formaldehyde solution. This pattern may also indicate of better preservation of glycogen with ethanol than with formalin. In addition, if bony tissues were included, the contrast result would be even more significant for I_2E; bony tissues have much higher grayscales than most soft tissues with I_2E treatment, while they fell with respect to soft tissues with I_2KI-formaldehyde (Fig. 1).

Simulations

By comparing simulation results of the two approaches, we found significant differences in the partition coefficients (K_d) and the retardation factors (R_t) of three tissues (skin, muscle, and fascia) between the I_2E and I_2KI-formaldehyde systems (Fig. 6; Table 2). The K_d of the same tissue modeled is always significantly higher in the I_2KI-formaldehyde system than in I_2E system. For instance, it is over three times higher for the skin, and over four times higher for the muscle and fascia of K_d in I_2E system compared to that in I_2KI-formaldehyde system. For retardation factors, they are all higher in I_2KI-formaldehyde system than in I_2E, the ratios are ranged from 2.8 to 3.6 for different tissues compared in the two systems. The modeling results are consistent with analyses of grayscales values, which indicate

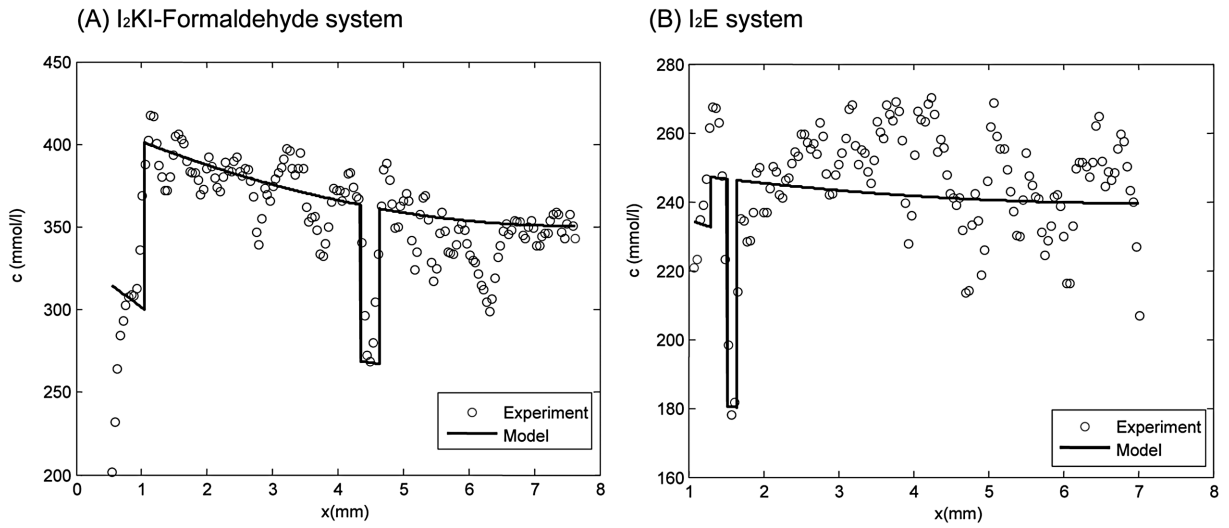

Figure 6. Experimental observations and model simulation results for iodine concentration changes across tissues within the cervical region. Simulation parameters for the I_2KI-formaldehyde and I_2E systems are provided in Table 2. See Supporting Information Material from where the experimental data were acquired.

the higher time efficiency for iodine species to diffuse in the I_2E system due to the larger effective diffusion coefficients for all tissues compared here. When comparing the K_d among different tissues using the same approach, K_d of muscle and fascia is greater than that of skin for both the I_2KI-formaldehyde and I_2E systems. Meanwhile, muscle and fascia has a similar R_t and much lower than that of skin in both the I_2KI and I_2E systems. Although the resulting boundary flux is greater in the I_2K system, significantly larger K_d and larger R_t for all three tissues in the simulation suggests that the transport of iodine into the inner region of muscle tissues is rather slow with I_2KI solution. This result is consistent with observations of chemical diffusion into soils, in which the larger the K_d the less mobile the chemical in soil solution (Strawn et al., 2015). Similarly, iodine is much more mobile in tissues with a lower K_d as suggested in the I_2E system. The higher flux in the simulation of the I_2KI-formaldehyde system (1–3%) is consistent with a higher iodine concentration used because flux is determined by solution concentration. The lower K_d for tissues in I_2E is also consistent with higher solubility of iodine in pure ethanol (Varlamova et al., 2009) than in aqueous solution.

Size Change

For the cephalic material, no significant differences in size or shape (e.g., via shrinkage) were observed due to staining based on comparison of lineal measurements for the same imaging location before and after staining. We ascribe this to the strong support of bony tissues within the cranial specimens, which restricted the potential shrinkage of soft tissues. Similar results have been reported for mounted whole bird specimens (Tahara and Larsson, 2013) and our previous results indicate minor shrinkage with longer staining duration on larger cranial specimens (Li et al., 2015). Less than 10% shrinkage in lineal measurements was observed for the tongue specimens after both I_2KI-formaldehyde and I_2E staining compared to the size before the staining (after fixation). The shrinkage of I_2E treated tongue is likely greater than I_2KI-formaldehyde due to the dehydrating effect of the more highly concentrated ethanol used.

DISCUSSION

Previous histological work has shown that fixation with NBF versus ethanol strongly affects the results of staining (Troiano et al., 2009). As an additive fixative, NBF stabilizes a wide array of tissues by forming binding and cross-linkages between proteins and nucleic acids (Hopwood, 2002; Carson and Hladik, 2009). In contrast, nonadditive ethanol-fixation mainly results in the coagulation of proteins by removing water from tissues (Hopwood, 2002). Better preservation of glycogen was reported for fixation using pure ethanol or alcoholic formalin, but it works poorly in preserving lipids (Carson and Hladik, 2009). Mechanical properties of bones have been noted as being significantly modified by both formalin fixation and ethanol fixation, but in different ways (Hammer et al., 2014). Pure ethanol has a major effect in weight reduction on bones through dehydration (Hammer et al., 2014). In comparison, structural modification by the formalin solution affects the organization of the organic matrix within bones and other tissues. This modification involved stronger cross-linking and binding within bony matrix

(Troiano et al., 2009; Hammer et al., 2014). Here, the reduced permeability of bone by iodine molecules is noted when using I_2KI-formaldehyde staining following formalin fixation. Ethanol fixation, on the other hand, may increase the permeability of bone and other tissues by increasing its porosity due to the dehydration. Thus, in addition to the distinct iodine species in the two solutions, other factors that influence the staining results include modifications of tissue density, porosity, permeability, and the fixed charge density of tissues during the fixation. Most of these parameters appear to evolve in a favorable way for iodine diffusion and staining under ethanol-based treatment.

As shown in other experiments, it seems to be more efficient to use I_2E staining, requiring relatively shorter staining durations even though the concentration adopted is usually lower than that of I_2KI (Metscher, 2009a,b; Degenhardt et al., 2010; Tahara and Larsson, 2013). The simulation results also provide a key to interpreting intrinsic differences between the two approaches. Under our simulation, tissues in the I_2E system all have lower K_d and R_t than in the I_2KI-formaldehyde system; this suggests a faster diffusion rate or more mobile iodine in the I_2E staining domain. Ethanol fixation and its further use as the solvent of iodine not only plays a role in removing water from tissues, but also increases the potential solubility of iodine elements within the solute phase of tissues, which leads to higher staining efficiency by reducing their K_d. In addition, the diffusion rate of pure ethanol itself is higher than aqueous formalin (Hopwood, 2002). Therefore, we consider the ethanol-based I_2E approach is likely to be more time efficient in staining most bird heads. However, caution should be taken because a larger degree of shrinkage and distortion in various tissues occurs with I_2E staining than I_2KI-formaldehyde when similar concentrations are used (Buytaert et al., 2014).

Fiber structures within muscles are better visualized in detail with I_2KI-formaldehyde treatment (Figs. 2 and 3). These subtle differences are likely due to extensive dehydration of tissues caused by ethanol (Figs. 2 and 4). Lower porosity and impermeability might be responsible for the low perviousness of cartilage and bone to iodine solution; however, via dehydration, I_2E staining significantly improves the contrast for bones but it is only slightly effective for cartilage (Fig. 1). The lack of a vascular system (blood vessels) and a dense triple-helical structure and high anionic fixed charge density (Hu and Athanasiou, 2003; Palmer et al., 2006) may be responsible for the low penetration of cartilage by the solution and low adsorption of iodine. The application of this finding is worth notice by researchers who are interested not only in soft tissue contrast but also in maintaining contrast between bone and soft tissue.

We did not explore the intrinsic differences for the results of the two solutions used; it should be considered that the I-I species (in I_2E solution) might have markedly different behavior from the I_3^- or I_5^- species (in I_2KI-formaldehyde solution). Sorption of iodine should be treated distinctively between the two as iodine species are different in the two solution (I_3^-, I_5^-, etc., vs. I-I). Differences in molecular weight, size, and polarity all could affect the staining results. The specific characteristics of these staining agents should be considered along with the tissue properties in order to define specific protocols in the future. In addition to the composition, structural differences, or how easily iodide species can penetrate and bind with tissues, other variables are worth further exploration to gain a better understanding of iodine sorption behaviors in different tissues. For instance, layered tissues, including muscles, lamina propria, and epithelia, are better stained than the denser, more amorphous tissues such as cartilage, which could potentially be caused by local anisotropy in tissue diffusivity.

Formaldehyde is known to react with dissolved iodine species, specifically triiodide, to produce the less-dense and colorless I^- ion. While the oxidation occur between the iodine species (I_3^-) and the small amount of formaldehyde in the NBF solution (i.e., as $HCHO + 3OH^- + I_3^- \longleftrightarrow HCOO^- + 3I^- + 2H_2O$), the requirement for the reaction to move toward the right is the presence of highly concentrated OH^- or at least a partially alkaline solution (Mei, '58). However, the NBF solution used here is only weakly alkaline or generally neutral (as the PH is around 7.2). Therefore, the concentration of OH^- is much lower than the active oxidation reaction requires. In addition, considering that the reaction is bidirectional, the large presences of I^- (from KI) in the system would meanwhile drive the reaction to move toward the left. This conclusion is supported by the color of the solution during the experiment, which is consistent with I_3^- and not I^- concentrated in the staining solution. In addition, extra potassium iodine (about three times the weight of iodine) adding in the system will help to maintain the fully dissolved iodine as triodine in the I_2KI-formaldehyde solution (Li, pers. obs.).

CONCLUSIONS

The nature of iodine binding with organic tissues is poorly understood for both I_2E and I_2KI staining, even though these solutions have been used in histology for decades (Gray, '54) and have more recently gained popularity for diceCT (Gignac et al., 2016). Here, we report evidence of several key differences in the behavior of tissues in reaction to distinct iodine solutions. The ethanol-based iodine-staining approach seems to be more time efficient in facilitating diffusion of iodine within major tissues than the aqueous formalin approach, a finding reinforced by simulations. Penetration and sorption of iodine into bones is much more effective in I_2E than in I_2KI-formaldehyde. The different results appear best explained by both differences in fixation, solvent, and the diffusion characteristics of distinct iodine species. For major soft tissue types, recovered variation in grayscale values tracks differences in glycogen concentrations. In general, the I_2E approach is better than I_2KI-formaldehyde for staining the avian cephalic samples investigated due to glycogen preservation in fixation, larger soft tissue grayscale contrast,

and effective staining of bony tissues. We note, however, that our results may not apply to the aqueous-I_2KI staining and further work is needed to test whether the pattern found here holds for the comparison of I_2KI aqueous versus I_2E staining.

ACKNOWLEDGMENTS

We thank T. Riede and F. Goller for help in acquiring the specimens, M.W. Colbert for discussion, and two referees for their valuable comments that significantly improved the manuscript. TNHC and VPL Facilities at The University of Texas at Austin are thanked for sample processing. Funding from the Gordon and Betty Moore Foundation (Grant No. 4498) and Jackson School of Geosciences, The University of Texas at Austin (to J.A.C. and Z.L.) is gratefully acknowledged. The University of Texas High-Resolution X-ray CT Facility is supported by NSF grant EAR-1258878 (to R.A.K. and J.A.M.).

LITERATURE CITED

Brobby GW. 1972. On the harderian gland of the domestic duck (*Anas platyrhynchus*). Cell Tissue Res 133:223–230.

Buytaert J, Goyens J, De Greef D, Aerts P, Dirckx J. 2014. Volume shrinkage of bone, brain and muscle tissue in sample preparation for micro-CT and light sheet fluorescence microscopy (LSFM). Microsc Microanal 20:1208–1217.

Carson FL, Hladik C. 2009. Histotechnology A self-instructional text, 3rd edition. American Society of Clinical Pathology.

Degenhardt K, Wright AC, Horng, D., Padmanabhan A, Epstein JA. 2010. Rapid 3D phenotyping of cardiovascular development in mouse embryos by micro-CT with iodine staining. Circ Cardiovasc Imag 3:314–322.

Gignac PM, Kley NJ. 2014. Iodine-enhanced micro-CT imaging: methodological refinements for the study of the soft-tissue anatomy of post-embryonic vertebrates. J Exp Zool B Mol Dev Evol 322:166–176.

Gignac PM, Kley NJ, Clarke JA, Colbert MW, Morhardt AC, Cerio D, Cost IN, Cox PG, Daza JD, Early CM, Echols MS, Henkelman RM, Herdina AN, Holliday CM, Li Z, Mahlow K, Merchant S, Müller J, Orsbon CP, Paluh DJ, Thies ML, Tsai HP, Witmer LM. 2016. Diffusible iodine-based contrast-enhanced computed tomography (diceCT): an emerging tool for rapid, high-resolution, 3-D imaging of metazoan soft tissues. J Anat 228:889–909. doi: 10.1111/joa.12449

Gray P. 1954. The microtomist's formulary and guide. New York & Toronto: The Blakiston Co.

Hammer N, Voigt C, Werner M, et al. 2014. Ethanol and formaldehyde fixation irreversibly alter bones' organic matrix. J Mech Behav Biomed Mater 29:252–258.

Hevor TK, Lehr PR, Gayet J. 1975. Amphetamine-induced changes in body temperature and glycogen content of the encephalon in the chicken. Experientia 31:674–676.

Holliday CM, Tsai HP, Skiljan RJ, George ID, Pathan S. 2013. A 3-D interactive model and atlas of the jaw musculature of *Alligator mississippiensis*. PLoS One 8:e62806.

Hopwood D. 2002 Fixation and fixatives. In: Gamble M, editor. Theory and practice of histological techniques, 5th edition. Bancroft JD: Elsevier Health Sciences. Edinburgh: Churchill Livingstone. p 63–84.

Hu JCY, Athanasiou KA. 2003 Structure and function of articular cartilage. In: An YH, Martin KL, editors. Handbook of histology methods for bone and cartilage. Totowa, NJ: Humana Press. p 73–95.

ICRP. 2009. Adult reference computational phantoms. ICRP Publication 110. Ann. ICRP 39:2.

Isacsson G, Mervyn S. 1981. Content and distribution of glycogen in oral epithelial dysplasia. Eur J Oral Sci 89:79–88.

Jeffery NS, Stephenson RS, Gallagher JA, Jarvis JC, Cox PG. 2011. Microcomputed tomography with iodine staining resolves the arrangement of muscle fibres. J Biomech 44:189–192.

Lecker DN, Kumari S, Khan A. 1997. Iodine binding capacity and iodine binding energy of glycogen. J Polymer Sci Polymer Chem 35:1409–1412.

Lewis S. 2004. Avian biochemistry and molecular biology. Cambridge: Cambridge University Press.

Li Z, Clarke JA, Ketcham RA, Colbert WM, Yan F. 2015. An investigation of the efficacy and mechanism of contrast-enhanced X-ray computed tomography utilizing iodine for large specimens through experimental and simulation approaches. BMC Physiol 15:5.

Mei H. 1958. Comparative experiments of iodimetric determination of glucose and formaldehyde. Chin Pharm J 6:284–284.

Metscher BD. 2009a. Micro-CT for comparative morphology: simple staining methods allow high-contrast 3-D imaging of diverse non-mineralized animal tissues. BMC Physiol 9:11.

Metscher BD. 2009b. Micro-CT for developmental biology: a versatile tool for high-contrast 3-D imaging at histological resolutions. Dev Dynam 238:632–640.

Palmer AW, Guldberg RE, Levenston ME. 2006. Analysis of cartilage matrix fixed charge density and three-dimensional morphology via contrast-enhanced microcomputed tomography. Proc Natl Acad Sci USA 103:19255–19260.

Palumbo G, Zullo F. 1987. The use of iodine staining for the quantitative analysis of lipids separated by thin layer chromatography. Lipids 22:201–205.

Riede T, Li Z, Tokuda IT, Farmer CG. 2015. Functional morphology of the *Alligator mississippiensis* larynx with implications for vocal production. J Exp Biol 218:991–998.

Schleip R, Müller DG. 2013. Training principles for fascial connective tissues: scientific foundation and suggested practical applications. J Bodyw Mov Ther 17:103–115.

Shackelford CD, Daniel DE. 1991. Diffusion in saturated soil. I: Background. J Geotech Eng 117:467–484.

Staedler YM, Masson D, Schönenberger J. 2013. Plant tissues in 3D via X-ray tomography: simple contrasting methods allow high resolution imaging. PLoS One 8:e75295.

Steiniche T, Hauge EM. 2003. Normal structure and function of bone. In: An YH, Martin KL, editors. Handbook of histology methods for bone and cartilage. Totowa, NJ: Humana Press. p 59–72.

Strawn DG, Bohn HL, O'Connor GA. 2015. Soil chemistry, 4th edition. Chichester, West Sussex, UK; Hoboken, NJ, USA: Wiley Blackwell.

Tahara R, Larsson HC. 2013. Quantitative analysis of microscopic X-ray computed tomography imaging: Japanese quail embryonic soft tissues with iodine staining. J Anat 223:297–310.

Troiano NW, Ciovacco WA, Kacena MA. 2009. The effects of fixation and dehydration on the histological quality of undecalcified murine bone specimens embedded in methylmethacrylate. J Histotechnol 32:27–31.

Varlamova TM, Rubtsova EM, Mushtakova SP. 2009. Solubility diagrams of the potassium iodide-water-ethanol and iodine-water-ethanol ternary systems. Russ J Phys Chem A 83:1896–1899.

Yan F, Chu Y, Zhang K, Tomson MB. 2015. Determination of adsorption isotherm parameters with correlated errors by measurement error models. Chem Eng J 281:921–930.

Yu X, Houtman C, Atalla RH. 1996. The complex of amylose and iodine. Carbohydr Res 292:129–141.

Zaidi Z, Lanigan SW. 2010. Dermatology in clinical practice. London: Springer.